

Rest-frame properties of 32 gamma-ray bursts observed by the *Fermi* Gamma-Ray Burst Monitor

D.Gruber¹, J. Greiner¹, A. von Kienlin¹, A. Rau¹, M. S. Briggs², V. Connaughton², A. Goldstein², A. J. van der Horst², M. Nardini¹, P. N. Bhat², E. Bissaldi¹, J. M. Burgess², V. L. Chaplin², R. Diehl¹, G. J. Fishman⁴, G. Fitzpatrick³, S. Foley¹, M. H. Gibby⁵, M. M. Giles⁵, S. Guiriec², R. M. Kippen⁶, C. Kouveliotou⁴, L. Lin², S. McBreen^{1,3}, C. A. Meegan⁷, F. Olivares E.¹, W. S. Paciesas², R. D. Preece², D. Tierney³, C. Wilson-Hodge⁴.

¹ Max Planck Institute for extraterrestrial Physics, Giessenbachstrasse 1, 85748, Garching, Germany
e-mail: dgruber@mpe.mpg.de

² University of Alabama in Huntsville, NSSTC, 320 Sparkman Drive, Huntsville, AL 35805, USA

³ University College, Dublin, Belfield, Stillorgan Road, Dublin 4, Ireland

⁴ Space Science Office, VP62, NASA/Marshall Space Flight Center Huntsville, AL 35812, USA

⁵ Jacobs Technology, Inc., Huntsville, Alabama

⁶ Los Alamos National Laboratory, P.O. Box 1663, Los Alamos, NM 87545, USA

⁷ Universities Space Research Association, NSSTC, 320 Sparkman Drive, Huntsville, AL 35805, USA

Preprint online version: October 19, 2018

ABSTRACT

Aims. In this paper we study the main spectral and temporal properties of gamma-ray bursts (GRBs) observed by *Fermi*/GBM. We investigate these key properties of GRBs in the rest-frame of the progenitor and test for possible intra-parameter correlations to better understand the intrinsic nature of these events.

Methods. Our sample comprises 32 GRBs with measured redshift that were observed by GBM until August 2010. 28 of them belong to the long-duration population and 4 events were classified as short/hard bursts. For all of these events we derive, where possible, the intrinsic peak energy in the νF_ν spectrum ($E_{p,\text{rest}}$), the duration in the rest-frame, defined as the time in which 90% of the burst fluence was observed ($T_{90,\text{rest}}$) and the isotropic equivalent bolometric energy (E_{iso}).

Results. The distribution of $E_{p,\text{rest}}$ has mean and median values of 1.1 MeV and 750 keV, respectively. A log-normal fit to the sample of long bursts peaks at ~ 800 keV. No high- E_p population is found but the distribution is biased against low E_p values. We find the lowest possible E_p that GBM can recover to be ≈ 15 keV. The $T_{90,\text{rest}}$ distribution of long GRBs peaks at ~ 10 s. The distribution of E_{iso} has mean and median values of 8.9×10^{52} erg and 8.2×10^{52} erg, respectively. We confirm the tight correlation between $E_{p,\text{rest}}$ and E_{iso} (Amati relation) and the one between $E_{p,\text{rest}}$ and the 1-s peak luminosity (L_p) (Yonetoku relation). Additionally, we observe a parameter reconstruction effect, i.e. the low-energy power law index α gets softer when E_p is located at the lower end of the detector energy range. Moreover, we do not find any significant cosmic evolution of neither $E_{p,\text{rest}}$ nor $T_{90,\text{rest}}$.

Key words. Gamma-ray burst: general

1. Introduction

Gamma-ray Bursts (GRB) are the most luminous flashes of γ -rays known to humankind. It is generally believed that they originate from a compact source with highly relativistic collimated outflows ($\Gamma > 100$).

A large fraction of our knowledge of the prompt emission comes from the Burst and Transient Explorer (BATSE, Meegan et al. 1992) onboard the Compton Gamma-Ray Observatory (*CGRO*, 1991-2000). Unfortunately, only a handful of BATSE bursts had a measured redshift because the BATSE error boxes were too large and thus, follow-up observations with X-ray and optical instrumentation was very limited. Moreover, the first afterglow was only detected in 1997, already near the end of the BATSE mission. The lack of distance measurements led to a focus of GRB studies in the observer frame without redshift corrections. Due to the cosmological origin of GRBs, such a correction is likely to be necessary to understand the intrinsic nature of these events.

With the two dedicated satellites, Beppo-SAX (Boella et al. 1997) and *Swift* (Gehrels et al. 2004), the situation has changed

and afterglow and host galaxy spectroscopy has provided redshifts for more than 200 events by now. Unfortunately, the relatively narrow energy band of Beppo-SAX (0.1 keV - 300 keV) and *Swift*/BAT (15 keV - 150 keV) limits the constraints on the prompt emission spectrum because the peak energy, E_p , in the νF_ν spectrum of GRBs, can only be determined for low E_p values and is often unconstrained (Butler et al. 2007; Sakamoto et al. 2009).

In this work we will take advantage of the broad energy coverage of the *Fermi*/GBM (8 keV - 40 MeV) to study the primary spectral and temporal properties, such as E_p , T_{90} , the time interval in which 90% of the burst fluence has been observed, and E_{iso} , the isotropic equivalent bolometric energy, in the rest-frame of the progenitors of 32 GRBs with measured redshift.

2. GRB sample and analysis

2.1. Instrumentation

The Gamma-Ray Burst Monitor (GBM) is one of the instruments onboard the *Fermi* Gamma-Ray Space Telescope

(Atwood et al. 2009) launched on June 11, 2008. Specifically designed for GRB studies, GBM observes the whole unocculted sky with a total of 12 thallium-activated sodium iodide (NaI(Tl)) scintillation detectors covering the energy range from 8 keV to 1 MeV and two bismuth germanate scintillation detectors (BGO) sensitive to energies between 150 keV and 40 MeV (Meegan et al. 2009). Thus, GBM offers a unprecedented view of GRBs, covering more then 3 decades in energy.

2.2. Burst selection

The selection criterion for our sample is solely based on the redshift determination. We form a sample of 32 bursts detected by GBM up to October 16th, 2010, with known redshift (determined either spectroscopically or photometrically).

Our sample contains 4 short and 28 long GRBs. The redshift distribution of the GBM GRBs is shown in Fig. 1 together with a histogram of all 239 GRBs with redshift determinations to date¹. A two-tailed Kolmogorov-Smirnov (KS) test between the full sample and the GBM-only sample shows that the two distributions are very similar ($P = 84\%$). In conclusion, the GBM-only sample is representative of the full GRB sample with redshift.

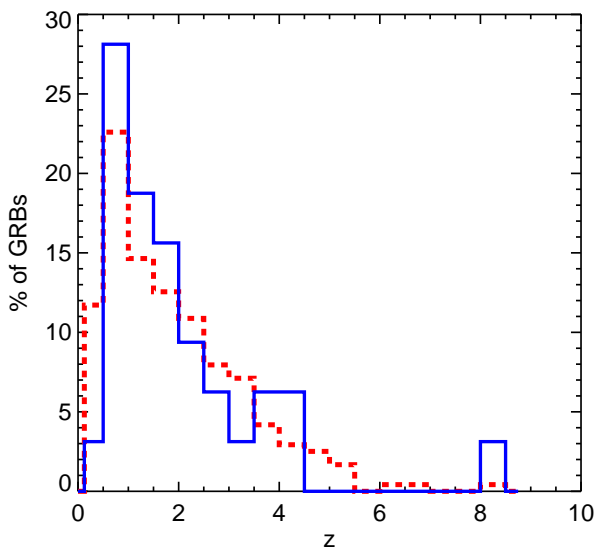


Fig. 1. Redshift distribution in % of GBM GRBs (blue solid line) compared to all 239 GRBs with measured redshift to date (red dashed line). Both samples contain long and short bursts.

2.3. Analysis of the GBM Data

For the E_p determination, CSPEC data (Meegan et al. 2009) with a time resolution of 1.024 s (4.096 s pre-trigger) were used. For the short GRBs, i.e. those with $T_{90} \leq 2$ s, time-tagged event (TTE, Meegan et al. 2009) data were used with a fine time resolution of 64 ms and the same channel boundaries as CSPEC data.

Detectors with source angles greater than 60° and those occulted by the spacecraft or solar panels were discarded. A maximum of three NaI detectors were used for each E_p determination. In four cases (GRB 090929A, GRB 090904B,

GRB 090618, and GRB 081007) only one NaI detector could be used due to the reasons mentioned above. Where possible, both BGO detectors were included in the analysis if they were not occulted by the satellite during the prompt emission. Even if there was no apparent signal in the BGOs, they can help to determine an upper limit of the GRB signal in the spectra.

The spectral analysis was performed with the software package RMFIT² (version 3.3rc8) and the GBM Response Matrices v1.8. To account for the changing orientation of the source with respect to the detectors caused by the slew of the spacecraft, the detector response matrices (DRM) were generated for every 2 degrees on the sky.

For each burst we fitted for every energy channel a low-order polynomial to a user defined background interval before and after the prompt emission and interpolated this fit across the source interval.

Three model fits were applied to all time bins with a signal-to-noise (S/N) of at least 3.5 above the background model: a single power-law (PL), a power law function with an exponential high energy cutoff (COMP) and the Band function (Band et al. 1993a). For three GRBs (GRB 090424, GRB 090618, and GRB 090926A) an effective area correction was applied to the BGO with respect to the NaI detectors to account for systematics which dominate the statistical errors due to the brightness of these events. The best model fit is the function which provides the best Castor C-stat value (Cash 1979). An improvement by $\Delta C\text{-stat} = 10$ for every degree of freedom is required. The profile of the Cash statistics was used to estimate the 1σ asymmetric error.

The values obtained with this analysis method may be superseded by the GBM spectral catalogue released by the GBM team (Goldstein et al., in preparation).

3. The intrinsic properties

3.1. The peak energy (E_p)

3.1.1. Instrumental bias

A first important issue which needs to be addressed is whether the bursts observed by GBM are drawn from the same distribution as the bursts which were observed by BATSE. Because of the broader sensitivity of GBM to higher energies, there could be a significant deviation towards higher E_p values. To answer this question, we use the BATSE catalogue³ from which we extract the E_p values which were obtained from the time averaged spectra (fluence spectral fits). Ignoring the power-law (PL), Gaussian Log and Smoothly Broken Power Law (SBPL) fits, we elected to the COMP model or Band function for the purpose of this test. We require $\Delta E_p/E_p \leq 0.4$ and the low-energy power-law index, α has an absolute error $\sigma_\alpha \leq 0.4$. GRBs which did not fulfill these criteria were rejected from the sample. The Band function was always preferred over the COMP model in cases in which the high-energy power-law index β was constrained ($\sigma_\beta < 0.4$). Both long and short GRBs were included in this analysis. The so obtained E_p distribution shown in Fig. 2.

The same selection cut was applied to the 2-year GBM spectral catalogue. The red histogram in Fig. 2 shows this distribution. Both distributions peak at ≈ 170 keV and show the same standard deviation. A KS test reveals that the difference

² RMFIT for GBM and LAT analysis was developed by the GBM Team and is publicly available at fermi.gsfc.nasa.gov/ssc/data/analysis/.

³ www.batse.msfc.nasa.gov/goldstein/

¹ www.mpe.mpg.de/~jcg/grbgen.html

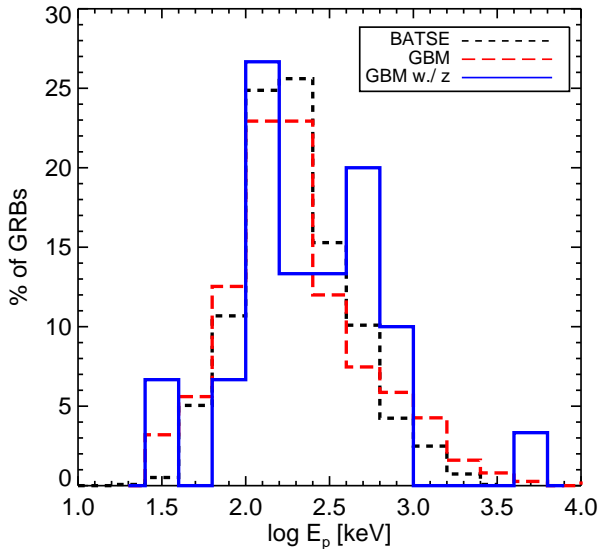


Fig. 2. E_p values of 1367 BATSE/CGRO GRBs with a log-normal fit (black dotted histogram and line), 375 GBM GRBs and log-normal fit (red dashed histogram and line) and 30 GBM GRBs with redshift measurement (blue solid histogram). A KS test suggests that all three samples were drawn from the same distribution.

between the two samples is not statistically meaningful ($P = 18\%$). This means that the two histograms are drawn from the same distribution, in agreement with Nava et al. (2010). We note that, Bissaldi et al. (2011) showed that the E_p distribution of some GBM-GRBs extends to higher energies compared to BATSE (Kaneko et al. 2006). However, this is of no surprise as Amati et al. (2002) demonstrated that bursts with higher fluence, i.e. higher E_{iso} , have, on average, higher E_p (see also Sect.4.1). Since Bissaldi et al. (2011) only use bright GRBs, it is to be expected that their E_p distribution is shifted to higher energies. We conclude that GBM, although being sensitive up to 40 MeV, does not find a previously undiscovered population of high- E_p GRBs, consistent with Harris & Share (1998).

The KS test was then applied to both the E_p distributions between the whole sample of GBM bursts and the 30 GBM bursts with measured redshift (for GRB 090519A and GRB 080928 a PL model fits the data best) and also to the E_p distribution of BATSE bursts and the E_p distribution of GBM bursts with measured redshift. In neither case the differences were statistically meaningful ($P = 24\%$ and $P = 20\%$, respectively). Thus, all 3 histograms are very likely drawn from the same distribution. In conclusion, the sample of GBM GRBs with measured redshift presented here is representative for the whole population of GRBs which were ever observed by BATSE and GBM.

However, it should be stressed that GBM cannot measure E_p values which are lower than a certain limiting threshold. It is well known that E_p values of GRBs can go as low as a few keV. Pélangéon et al. (2008) for example find E_p values as low as ~ 2 keV in GRBs that were observed by the High Energy Transient Explorer 2 (*HETE-2*, see e.g. Barraud et al. 2003 and references therein). These low energetic events have been classified as X-ray flashes (XRF) or X-ray rich bursts (XRB) (see e.g. Heise & in 't Zand 2001; Sakamoto et al. 2005). However, it is very likely that XRFs and XRBs are nothing else than weak and long GRBs (see Kippen et al. 2004, and references therein).

The borderline E_p value is obviously located somewhere near the low-energy sensitivity of the NaIs, which has yet to be determined. Thus, in order to determine a potential bias in the $E_{p,\text{rest}}$ distribution shown in Fig. 3, it is important to understand and quantify the limits of the GBM to measure E_p (be it either from the COMP model or Band function).

For this purpose, we created a set of simulated bursts with different initial spectral and temporal starting values. We input the source lifetime (t_s , 1 s, 5 s, 10 s, 100 s) and the photon flux (f) in the 10 keV to 1 MeV range (1, 3 and 10 ph cm $^{-2}$ s $^{-1}$). For the simulation the Band function was chosen as the photon model with varying E_p (15, 17, 25, 50, 100 keV) but fixed $\alpha = -0.8$ and $\beta = -2.4$. We simulate these bursts overlaid on real background data by using detector NaI 7 of GRB 090926A⁴. This results in 60 different burst models. For each model, we created 1000 bursts to account for Poissonian noise. This results in 60000 spectra, each of which was then fitted with the Band function using the detector response matrix (DRM) of detector NaI 7 created for the location of GRB 090926A.

After the fitting procedure, we reject those bursts which have $\Delta E_p/E_p \geq 0.3$ and $\sigma_\alpha \leq 0.4$. These rejected spectra are then defined as unconstrained. We did not apply this criterion to the high-energy power law index β . A spectral fit that has a constrained E_p and α but an unconstrained β is simply considered a COMP model. In Table 1 we report the mean and standard deviation of the output spectral parameters, E_p and α , of the simulated bursts.

The conclusions of this exercise are:

1. GBM can recover E_p values only as low as ≈ 15 keV. The fact that the observed E_p distribution is indeed biased is in clear contradiction to e.g. Brainerd et al. (2000). They argued that the observed E_p distribution (by BATSE in this case) is actually the intrinsic one.
2. the input E_p parameter can be recovered from the simulated spectra within the 2σ errors for almost all simulated flux levels and source lifetimes.
3. GRBs with low fluxes, low E_p and short t_s are more likely to be rejected than GRBs with higher fluxes, higher E_p or longer t_s .
4. the low-energy power law index α tends to get softer, i.e. to have lower values, for low E_p and low fluxes. This last point is particularly noteworthy. Crider et al. (1997), Lloyd-Ronning & Petrosian (2002) and later Kaneko et al. (2006) found a significant correlation between E_p and α in the time-resolved spectra of several GRBs. Supported by our simulations, we point out the possibility that a parameter reconstruction effect is at work in addition to any intrinsic correlation between E_p and α . This effect has already been brought forward by Preece et al. (1998); Lloyd & Petrosian (2000) and Lloyd-Ronning & Petrosian (2002). In short, it depends on how quickly α can reach its asymptotic value and how close E_p is located to the low-energy limit of the instrument's energy bandpass. The closer E_p is situated to the detector's sensitivity limit, the fewer is the number of photons in the low-energy portion of the spectrum. This makes it increasingly difficult to determine the asymptotic value of α . Instead, a more negative value of the low-energy power law index will be measured which is what is observed here.

⁴ The choice of NaI 7 and the choice for this specific GRB is completely arbitrary. We could have chosen any other detector that observed any other real GRB.

Table 1. Mean and standard deviation of the output spectral parameters of the simulated bursts.

t_S	$E_{p,\text{in}}$	f	$E_{p,\text{out}}$	α_{out}	rej
10	15	10	$15.0^{+1.5}_{-1.4}$	-1.53 ± 0.36	98
100	15	1	$21.7^{+4.0}_{-3.4}$	-1.55 ± 0.16	99
100	15	3	$15.4^{+1.9}_{-1.7}$	-1.39 ± 0.30	92
100	15	10	$14.1^{+0.5}_{-0.5}$	-0.79 ± 0.16	46
1	17	3	$22.6^{+3.2}_{-2.8}$	-1.48 ± 0.25	96
1	17	10	$23.5^{+4.8}_{-4.0}$	-1.48 ± 0.20	97
5	17	3	$25.8^{+5.8}_{-4.7}$	-1.49 ± 0.18	99
5	17	10	$18.2^{+2.4}_{-2.1}$	-1.44 ± 0.23	88
10	17	3	$21.2^{+6.5}_{-5.0}$	-1.55 ± 0.17	93
10	17	10	$17.6^{+1.7}_{-1.6}$	-1.26 ± 0.27	79
100	17	1	$22.5^{+2.1}_{-1.9}$	-1.33 ± 0.23	96
100	17	3	$16.9^{+1.7}_{-1.6}$	-1.28 ± 0.25	39
100	17	10	$17.0^{+0.4}_{-0.4}$	-0.80 ± 0.12	0
1	25	10	$30.6^{+5.1}_{-4.4}$	-1.30 ± 0.28	86
5	25	3	$33.9^{+6.8}_{-5.6}$	-1.44 ± 0.24	96
5	25	10	$26.2^{+2.0}_{-1.9}$	-0.92 ± 0.29	39
10	25	3	$30.3^{+4.4}_{-3.8}$	-1.29 ± 0.27	80
10	25	10	$25.4^{+1.7}_{-1.6}$	-0.89 ± 0.25	4
100	25	1	$29.4^{+3.7}_{-3.3}$	-1.24 ± 0.27	73
100	25	3	$25.3^{+1.6}_{-1.5}$	-0.85 ± 0.24	1
100	25	10	$25.1^{+0.6}_{-0.6}$	-0.82 ± 0.11	0
1	50	10	$53.3^{+8.4}_{-7.2}$	-0.88 ± 0.28	52
5	50	3	$57.1^{+9.0}_{-7.8}$	-0.96 ± 0.27	62
5	50	10	$49.9^{+5.8}_{-5.2}$	-0.78 ± 0.22	0
10	50	3	$51.9^{+7.3}_{-6.4}$	-0.82 ± 0.29	37
10	50	10	$50.0^{+4.1}_{-3.8}$	-0.78 ± 0.16	0
100	50	1	$50.3^{+7.2}_{-6.3}$	-0.80 ± 0.28	21
100	50	3	$49.9^{+3.5}_{-3.3}$	-0.78 ± 0.14	0
100	50	10	$50.0^{+1.3}_{-1.3}$	-0.80 ± 0.05	0
1	100	3	$121.0^{+5.4}_{-5.2}$	-0.82 ± 0.13	99
1	100	10	$92.0^{+18.9}_{-15.7}$	-0.71 ± 0.25	16
5	100	3	$98.7^{+21.5}_{-17.7}$	-0.74 ± 0.26	21
5	100	10	$98.6^{+11.2}_{-10.1}$	-0.78 ± 0.13	0
10	100	3	$95.0^{+19.3}_{-16.0}$	-0.73 ± 0.23	4
10	100	10	$99.0^{+8.4}_{-7.7}$	-0.79 ± 0.09	0
100	100	1	$92.4^{+17.3}_{-14.6}$	-0.71 ± 0.23	8
100	100	3	$99.9^{+7.1}_{-6.6}$	-0.80 ± 0.08	0
100	100	10	$99.9^{+2.4}_{-2.4}$	-0.80 ± 0.03	0

Notes. This Table shows the input source lifetime, t_S (in s), $E_{p,\text{in}}$ (in keV), photon flux, f (in $\text{ph cm}^{-2} \text{s}^{-1}$), the recovered E_p , $E_{p,\text{out}}$ (in keV), the recovered low-energy PL index, α , and the percentage of bursts which were rejected due to the selection cut, rej (in %). The input low-energy power law index was -0.8 . Cases for which all simulated bursts were rejected are not reported in this Table (for details see text).

3.1.2. The intrinsic E_p distribution

In Fig. 3 we present a histogram of $E_{p,\text{rest}}$ of our sample of GBM GRBs where a E_p measurement was possible. The distribution of all bursts has mean and median values of 1.1 MeV and 750 keV, respectively. A log-normal fit to the sample of long

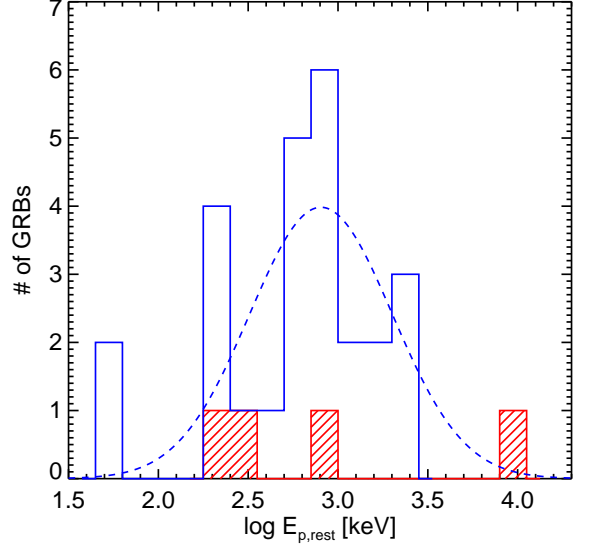


Fig. 3. Rest-frame distribution of E_p for 4 short (hatched histogram) and 26 long (empty histogram) GBM-GRBs. For two GRBs (GRB 090519A, GRB 080928) a simple PL model fits the data best, thus not providing an E_p value. The complete distribution has mean and median values of 1.1 MeV and 750 keV, respectively. A log-normal fit to the sample of long GRBs (dashed line) peaks at ~ 800 keV and has a FWHM = 0.93 in log-space.

bursts peaks at ~ 800 keV. In the canonical scenario of GRB jets, turbulent magnetic fields build up behind the internal shock, and electrons produce a synchrotron power law spectrum. The typical rest-frame frequency ν_{rest} in the internal shock dissipation is $\nu_{\text{rest}} \propto 0.2 L_{52}^{1/2} r_{13}^{-1} \text{MeV}$ (Zhang & Mészáros 2002), where L_{52} is the luminosity in 10^{52} erg/s and r_{13} the dissipation radius in units of 10^{13} cm. Our measurement of the rest-frame peak energy therefore leads to a constraint of $L_{52}^{1/2} r_{13}^{-1} \approx 0.8$ (in the above units).

Recently, Collazzi et al. (2011) reported that the width of the $E_{p,\text{rest}}$ distribution must be close to zero with the peak value located close to the rest-mass energy of electrons at 511 keV. This effectively implies that all GRBs must be thermostated by some unknown physical mechanism. We tested this claim by determining the width of the $E_{p,\text{rest}}$ distribution ($\sigma_{E_p(1+z)} = 0.48$) together with all the individual errors that add to the uncertainty of the E_p measurement in log-space (for details refer to eq. 1 in Collazzi et al. 2011):

$$\sigma_{\text{Total}}^2 = \sigma_{\text{Poisson}}^2 + \sigma_{\text{Det}}^2 + \sigma_{\text{Choice}}^2 + \sigma_{\text{Def}}^2. \quad (1)$$

σ_{Choice} describes the different choices made by different analysts. Since all the bursts in this paper were analyzed consistently (selection of the time interval, energy range, etc.), we can set $\sigma_{\text{Choice}} = 0$. σ_{Det} is the error which results in not knowing the detector response perfectly. However, according to Collazzi et al., σ_{Det} is negligibly small, meaning that the calibrations of the detectors are usually well understood. σ_{Def} describes the differences that are obtained in E_p when using different photon models. As it was shown already by e.g. Band et al. (1993b) and Kaneko et al. (2006) the COMP model results in higher E_p values than the Band function. Collazzi et al. use $\sigma_{\text{Model}} = 0.12$ to account for this difference. Here, this value is adopted as σ_{Def} .

The Poissonian errors are $\sigma_{\text{Poisson}} \approx 0.10$ in log-space. Thus

$$\sigma_{\text{Total}} = \sqrt{0.12^2 + 0.1^2} = 0.16.$$

Inserting the just found values in eq. 8 in Collazzi et al. gives

$$\sigma_{E_p^{\text{int}}}^2 = \sigma_{E_p(1+z)}^2 - \sigma_{\text{Total}}^2 = 0.45. \quad (2)$$

However, a zero width in the E_p distribution is synonymous with $\sigma_{E_p^{\text{int}}} = 0$. The conclusion is that the $E_{p,\text{rest}}$ distribution does not have a zero width. This finding is in conflict with the implications and conclusions discussed in Collazzi et al.

3.2. GRB duration (T_{90})

For determining the duration of a GRB, we applied the method first introduced by Kouveliotou et al. (1993). They defined the burst duration as the time in which 90% of the burst counts is collected (T_{90}). Here, we adopted the same definition; however, the burst's fluence was used instead of the counts. The T_{90} value depends highly on the detector and on the energy interval in which it is determined (see e.g. Bissaldi et al. 2011). Additionally, since we are interested in durations in the rest-frame of the GRB, it is not sufficient to simply account for the time dilation due to cosmic expansion by dividing the measured durations by $(1+z)$. The energy band in which the T_{90} is determined needs to be redshift corrected as well. We determine the burst duration in fluence space in the rest-frame energy interval from 50 keV to 300 keV, i.e. in the observer frame energy interval from $50/(1+z)$ keV to $300/(1+z)$ keV.

3.2.1. The intrinsic T_{90} distribution

In Fig.4 we present the rest-frame distribution of T_{90} of our sample of 32 GBM GRBs. The number of short bursts is still too small to unambiguously recover a bimodal distinction of short and long events in the rest-frame. Henceforth, a distinction is made between the short and long class of GRBs using an ad-hoc definition of $T_{90,\text{rest}} \leq 2$ s for short bursts and $T_{90,\text{rest}} > 2$ s for long bursts, although we do have neither observational nor physical evidence to support such a distinction in the GRB sample presented here. All GRBs in our sample that are defined as short in the observer-frame, also remain short with the here adopted definition. We note that GRB 100816A is peculiar in that it is classified as a short burst by GBM data, but it has a $T_{90} = 2.9 \pm 0.6$ in the 15 keV - 350 keV energy range in *Swift* data with a low-level emission out to about T_0+100 (Markwardt et al. 2010).

The mean value of the whole $T_{90,\text{rest}}$ distribution is 32.4 s and the median value is 10.8 s.

3.3. Isotropic energy (E_{iso})

E_{iso} is calculated by

$$E_{\text{iso}} = \frac{4\pi d_L^2}{1+z} S_\gamma, \quad (3)$$

where d_L is the luminosity distance and S_γ the fluence in the $1/(1+z)$ keV to $10/(1+z)$ MeV frame. We determine S_γ using the energy flux provided by the best-fit spectral parameters and multiplying it with the total time interval over which the fit was performed. Since we performed the fit for time intervals where the count rate exceeded a S/N ratio of 3.5, it happened that some time intervals of some bursts were not included in the fit (e.g. phases of quiescence where the count rate dropped back

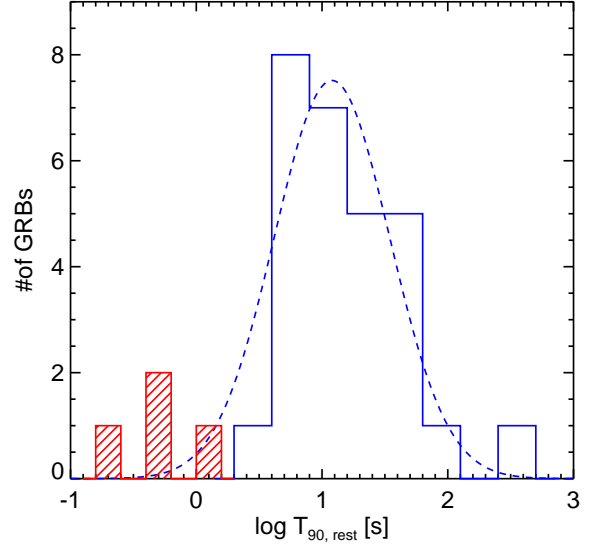


Fig. 4. $T_{90,\text{rest}}$ distribution of 4 short (red hatched histogram) and 28 long (blue histogram) GBM GRBs in the redshift corrected energy interval from 50 keV to 300 keV. The log-normal fit to the distribution (dashed line) of the long bursts peaks at ~ 12 s and has a FWHM = 1.1 in log-space.

to the background level). These time intervals were not used to calculate the fluence. The S_γ distribution is shown in Fig.5. The median value of the fluence distribution is 1.6×10^{-5} erg cm^{-2} and the mean value is 5.9×10^{-5} erg cm^{-2} . A log-normal fit to the data peaks at 2.2×10^{-5} erg cm^{-2} .

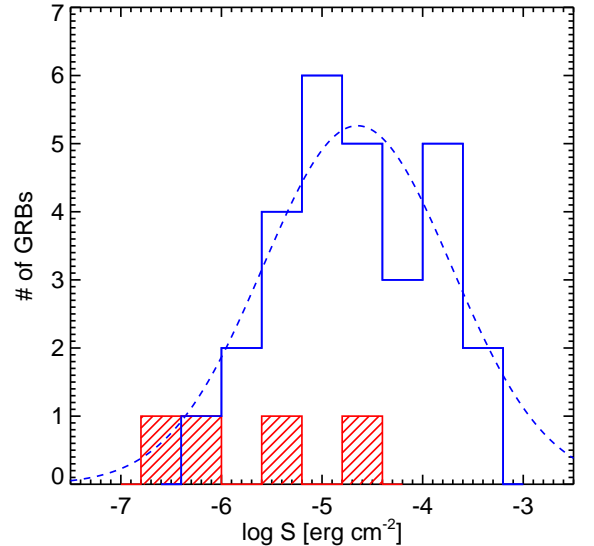


Fig. 5. Energy fluence distribution of 32 GBM GRBs determined in the energy range between $1/(1+z)$ keV to $10/(1+z)$ MeV range. The complete distribution has mean and median values of 1.6×10^{-5} erg cm^{-2} and 5.9×10^{-5} erg cm^{-2} . A log-normal fit (dashed line) to the long GRBs peaks at 2.2×10^{-5} erg cm^{-2} and has a FWHM = 2.2 in log-space.

The E_{iso} distribution is shown in Fig.6. The distribution for the long bursts has a median and mean value of 1.2×10^{53} erg and 1.4×10^{53} erg, respectively. Short bursts, on the other hand, have significantly lower values of 2.9×10^{51} erg and 4.0×10^{51} erg, respectively. A log-normal fit to the long bursts reveals a central value of $10^{53.1}$ erg. Because our sample is dominated by long GRBs a log-normal fit to the whole distribution results in an essentially unchanged peak value (10^{53} erg).

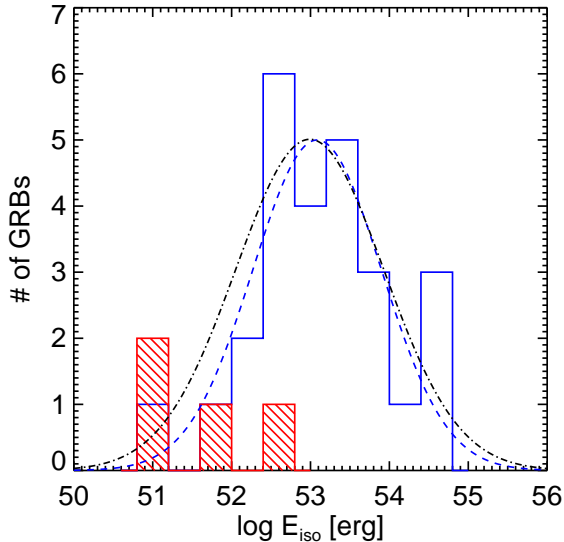


Fig. 6. E_{iso} distribution for long (blue hatched histogram) and short (red hatched histogram). For long bursts the distribution has mean and median values of 1.4×10^{53} erg and 1.2×10^{53} erg, respectively. A log-normal fit to the long bursts (dashed line) peaks at 1.2×10^{53} erg with a FWHM = 1.9 in log-space. Short bursts have a mean and median value of 4×10^{51} erg and 2.9×10^{51} erg, respectively. A log-normal fit to the combined sample (dash-dotted line) peaks at 9.8×10^{52} erg with a FWHM = 2.2 in log-space.

4. Correlations

4.1. Amati relation

Amati et al. (2002) first showed that there is a tight correlation between $E_{\text{p,rest}}$ and E_{iso} (the isotropic equivalent bolometric energy determined in the energy range between 1 keV to 10 MeV). This relation is now known as the ‘‘Amati relation’’. In Fig.7 we show the Amati relation for the 30 GBM GRBs with measured $E_{\text{p,rest}}$ and E_{iso} . While there is an evident correlation between these two quantities (Spearman’s rank correlation of $\rho = 0.74$ with a chance probability of 1.7×10^{-5}) the extrinsic scatter of the long GRBs is larger by a factor of ~ 2 in log-space compared to Amati (2010). Also, the best fit to our data is shifted to slightly larger $E_{\text{p,rest}}$ values. The best fit power-law index to the long GRBs of our sample is 0.52 ± 0.06 which is in agreement with the indices obtained by e.g. Amati (2010); Ghirlanda et al. (2009, 2010). As has been shown by other authors in the past (see e.g. Amati et al. 2008; Ghirlanda et al. 2009; Amati 2010) short bursts do not follow the relation, being situated well outside the 2σ scatter around the best-fit. This is true also for the power-law fit derived here (see Fig.7) except for GRB 100816A.

However, as already stated above this burst may actually fall in an intermediate or hybrid class of short GRBs with extended emission (see e.g. Norris & Bonnell 2006; Zhang et al. 2009).

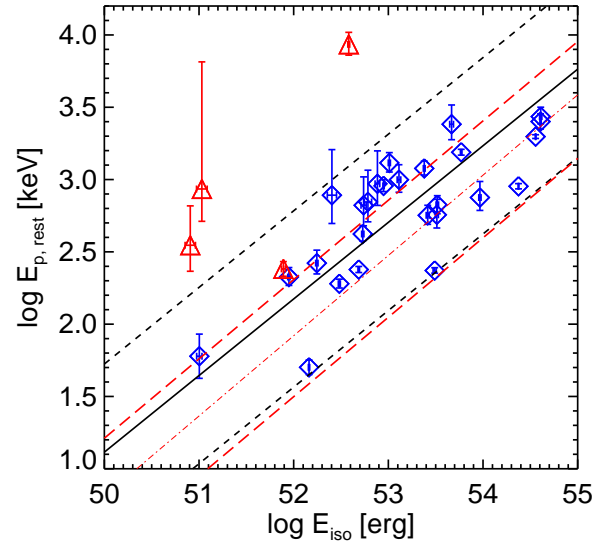


Fig. 7. Amati relation for 4 short (red open triangles) and 26 long (blue open diamonds) GBM GRBs. Also shown is the best power-law fit to the data (black solid line) and the extrinsic 2σ scatter (black dashed lines) with the best power-law fit published by Amati (2010) (red dash-dotted line) with the 2σ scatter (red long dashed line).

4.2. Yonetoku relation

Yonetoku et al. (2004) found a tight correlation between the rest frame peak energy in the νF_ν spectrum $E_{\text{p,rest}}$ and the 1-s peak luminosity (L_p) in GRBs (so called Yonetoku relation). The peak luminosity is calculated with

$$L_p = 4\pi d_l^2 F_p, \quad (4)$$

where d_l is the luminosity distance and F_p the 1 s peak energy flux. We determine F_p in the energy range between 30 keV and 10 MeV in the rest frame of the GRB (Yonetoku et al. 2004). We use the GBM peak spectral catalogue (Goldstein et al. 2011) to determine the best fit spectral parameters of the brightest 1 s bin. We then determined the energy flux in the rest-frame of the GRB by integrating

$$F = \int_{30/(1+z)}^{10000/(1+z)} N_0 E \Phi(E) dE, \quad (5)$$

where N_0 is the normalization of the spectrum (in photons $\text{cm}^2 \text{s}^{-1}$), E the energy and $\Phi(E)$ the form of the spectrum (either Band or COMP). In order to determine the error on the energy flux, we calculate 1000 flux values for each GRB by varying the input parameters, N_0 , E_p , α and β according to the 1σ error on each parameter. We then use the median and the mean absolute deviation (MAD) around the median of the 1000 simulated bursts to determine the peak energy flux and the error on the latter, respectively.

We present this relation for 30 GBM GRBs in Fig. 8 and find a best-fit power law index of 0.58 ± 0.08 . The Spearman's rank correlation gives $\rho = 0.7$ with a chance probability of 2.3×10^{-5} . Our findings are in good agreement with Yonetoku et al. (2004); Ghirlanda et al. (2009) and Ghirlanda et al. (2010).

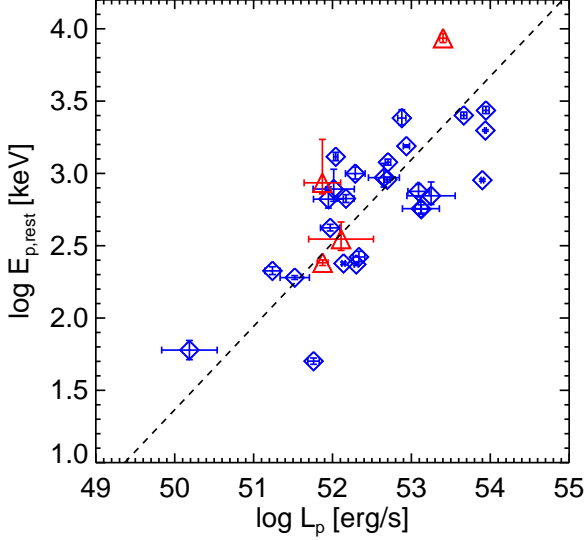


Fig. 8. Yonetoku relation for 4 short (red open triangles) and 26 long (blue open diamonds) GBM GRBs. Also shown is the best power-law fit to the data (black dashed line).

4.3. $T_{90,rest}$ vs redshift

The rest-frame T_{90} is plotted as a function of redshift in Fig. 9. Contrary to Pélagion et al. (2008), who find a negative correlation between $T_{90,rest}$ and z , we do not find any evidence in the GBM data for such a correlation. Also, there is no correlation between $T_{90,rest}$ and z when accounting for $E_{p,rest}$. A Spearman rank test for all bursts gives a correlation coefficient of $\rho = 0.04$ with a chance probability of $P = 0.81$. However, the p-value in Pélagion et al. is $\approx 10^{-3}$ which makes it a weak case for such a correlation in the first place. Our results confirm the analyses with *Swift* detected GRBs (Greiner 2011). We do note a lack of short GRBs for $z \geq 2$. This, however, is very likely a selection bias, because firstly, short GRBs at such high redshifts must be very luminous to be observed by GBM and secondly, short GRBs are subluminal in the optical band (Kann et al. 2008) and therefore it is difficult to obtain a redshift measurement.

4.4. $E_{p,rest}$ vs redshift

In order to explain the detection rate of GRBs at high- z , Salvaterra & Chincarini (2007) conclude that high- z GRBs must be more common (e.g. Daigne et al. 2006; Wang & Dai 2011) and/or intrinsically more luminous (Salvaterra et al. 2009) than bursts at low- z (but see Butler et al. 2010). As already mentioned above, Yonetoku et al. (2004) found a tight correlation between the 1-s peak-luminosity (L_p) and $E_{p,rest}$ in GRBs. Assuming that the luminosity function of GRBs indeed evolves with redshift and that the Yonetoku relation is valid, we would also expect a positive correlation of $E_{p,rest}$ with z .

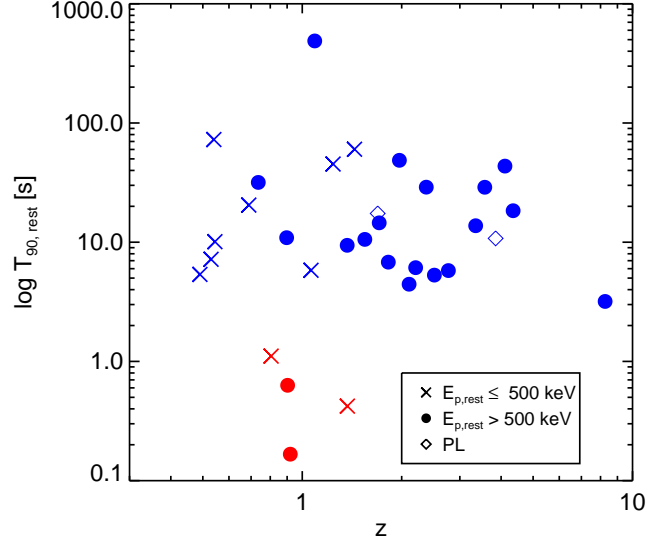


Fig. 9. Testing the cosmic evolution of $T_{90,rest}$. No correlation is evident. Bursts with $E_{p,rest} \leq 500$ keV are shown as crosses, bursts with $E_{p,rest} > 500$ keV shown as filled circles. The two bursts for which are best fit by a simple power-law are shown as open diamonds.

In Fig.10 we present $E_{p,rest}$ vs z . As was shown in Sect.3.1.1 and in Table 1, GBM can reliably measure E_p down to ~ 15 keV. The solid line indicates this redshift-corrected lower limit. The Spearman's rank correlation, using only the long GRBs, is $\rho = 0.58$ with a chance probability of $P = 2 \times 10^{-3}$. When including the short GRBs, the correlation coefficient effectively remains unchanged, whereas the chance probability increases to $P = 4 \times 10^{-3}$, making a correlation slightly less likely.

However, this correlation can be explained entirely by selection effects: GRBs do not populate the empty area in Fig. 10 (low $E_{p,rest}$ and $z > 1$) because they simply can not be detected by GBM. Even though GBM *could* recover a low E_p value of such GRBs, as was shown above, the detection of such events is very challenging because of the low photon fluxes of these events. As one can see in Fig.10 the lower boundary of the apparent correlation is composed of the bursts that have relatively low peak photon fluxes. This is already an indication that these events reside at the lower fluence limit for GBM to both trigger on these events.

Since we actually know the intrinsic parameters of the 32 GRBs, one can test up to which maximum redshift, z_{max} these bursts could have been detected, i.e. for which GBM would have triggered. GBM has many trigger algorithms (various trigger time scales for various energy ranges). For the purpose of this test, we focus on the 50 keV to 300 keV range which is the classical trigger energy range for a GRB and a timescale of a maximum of 4.096 s for long GRBs and 1.024 s for short GRBs. In order to shift a GRB to a higher redshift, three observables change:

1. The duration $T_{90}(z_{max}) = T_{90}(z_0) \frac{1+z_{max}}{1+z_0}$
2. The peak energy $E_p(z_{max}) = E_p(z_0) \frac{1+z_0}{1+z_{max}}$
3. The flux of the GRB.

While it is straightforward to account for the changes of E_p and T_{90} , the proper treatment of the flux is more complex. RMFIT outputs the spectral parameters, including the normal-

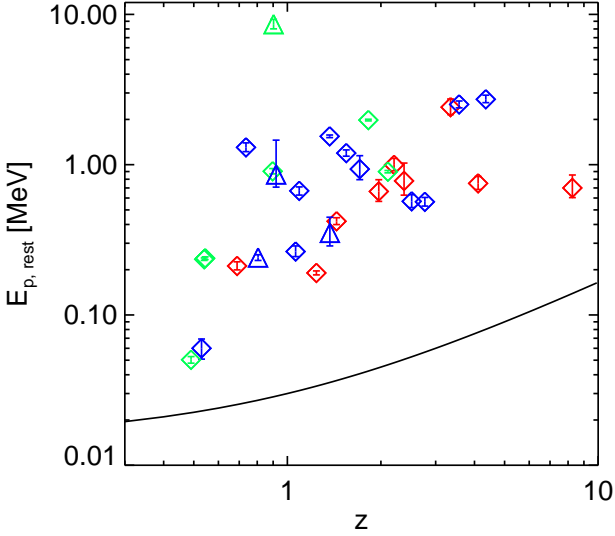


Fig. 10. Testing the cosmic evolution of $E_{p,\text{rest}}$ for long (diamonds) and short (triangles) GRBs. The solid line indicates the redshift corrected lower limit for GBM to measure E_p which is currently estimated to be ~ 15 keV in the observer frame (see Table 1). Bursts with high (green), intermediate (blue) and low (red) peak photon flux (in $\text{ph cm}^{-2} \text{s}^{-1}$) are labeled.

ization (N_0 in $\text{ph cm}^{-2} \text{s}^{-1} \text{keV}^{-1}$) of the spectrum, which can be recognized as a proxy for the flux of a GRB. Therefore, in order to decrease the flux when shifting the GRB to ever higher redshifts, the normalization has to be decreased accordingly. This was done as follows:

The photon luminosity of a GRB, in the energy band from E_1 to E_2 is defined as follows

$$L = 4\pi d_L^2 \int_{E_1/(1+z_0)}^{E_2/(1+z_0)} N_0 \Phi_1(E) dE, \quad (6)$$

where d_L is the luminosity distance and z_0 the redshift of the burst. The integral describes the photon flux of the burst in the E_1 to E_2 energy range at the rest-frame of the burst. N_0 is the normalization of the spectrum and $\Phi_1(E)$ is the shape of the spectrum (Band or COMP) with $E_p = E_p(z_0)$, i.e. $\Phi_2 = \Phi_2(E, E_p(z_0))$. The luminosity of a burst is independent of redshift. This, in turn, means that the above equation is valid also when exchanging z_0 with z_{max} . One gets

$$L = 4\pi d_L^2 \int_{E_1/(1+z_{\text{max}})}^{E_2/(1+z_{\text{max}})} N_{z_{\text{max}}} \Phi_2(E) dE, \quad (7)$$

where $\Phi_2 = \Phi_2(E, E_p(z_{\text{max}}))$.

Setting the two equations equal and solving for $N_{z_{\text{max}}}$ one is left with

$$N_{z_{\text{max}}} = N_0 \times \frac{d_{L,z_0}^2}{d_{L,z_{\text{max}}}^2} \times \frac{\int_{E_1/(1+z_0)}^{E_2/(1+z_0)} \Phi_1(E, E_p(z_0)) dE}{\int_{E_1/(1+z_{\text{max}})}^{E_2/(1+z_{\text{max}})} \Phi_2(E, E_p(z_{\text{max}})) dE}. \quad (8)$$

It can be shown, for both the COMP model and the Band function, that the fraction of the two integrals is nothing else than

$$\frac{\int_{E_1/(1+z_0)}^{E_2/(1+z_0)} \Phi_1(E, E_p(z_0)) dE}{\int_{E_1/(1+z_{\text{max}})}^{E_2/(1+z_{\text{max}})} \Phi_2(E, E_p(z_{\text{max}})) dE} = \frac{(1+z_{\text{max}})^{\alpha+1}}{(1+z)^{\alpha+1}}, \quad (9)$$

where α is the low-energy power law index.

Thus,

$$N_{z_{\text{max}}} = N_0 \times \frac{d_{L,z_0}^2}{d_{L,z_{\text{max}}}^2} \times \frac{(1+z_{\text{max}})^{\alpha+1}}{(1+z)^{\alpha+1}}. \quad (10)$$

For GBM to trigger, two detectors need to be above the trigger threshold. Therefore, real background information of the second brightest detector of every burst was used. With this background data, we shift each bursts in steps of $\Delta z = 0.25$ to higher redshifts and simulate 1000 bursts for each redshift step (changing the source lifetime, input E_p and normalization as described above, additionally adding Poissonian noise to the best-fit parameters) by forward folding the photon model through the detector response matrix, created at the time and location of the real GRBs. To determine if GBM would have triggered, we determine the signal-to-noise ratio (SNR) with

$$\text{SNR} = \frac{\Delta t \cdot c_s - \Delta t \cdot c_b}{\sqrt{\Delta t \cdot c_b}}, \quad (11)$$

where, Δt is the trigger time scale ($\Delta t = 4.096$ s for long GRBs and $\Delta t = 1.024$ s for short GRBs), c_s and c_b are the counts/s of the source and background, respectively. If more than 90% of the simulated bursts have $\text{SNR} \geq 4.5$ it can safely be assumed that the burst would have been detected at this redshift. We plot $E_{p,\text{rest}}$, which obviously remains constant at all redshifts, vs the range of the actually measured to maximum redshift in Fig. 11. We already know that the here presented sample of GRBs is representative of all bursts detected by GBM (see Sect. 3.1.1). Therefore, we note that the determination of the lowest measurable E_p value is not as crucial as the determination of the detector sensitivity. None of the bursts in our sample populates the empty region at $2 \leq z \leq 8$ and $50 \leq E_{p,\text{rest}} [\text{keV}] \leq 500$ even when shifting them at their maximum detectable redshift. We conclude that the correlation between $E_{p,\text{rest}}$ and z can be explained entirely by the sensitivity limitations of the instrument.

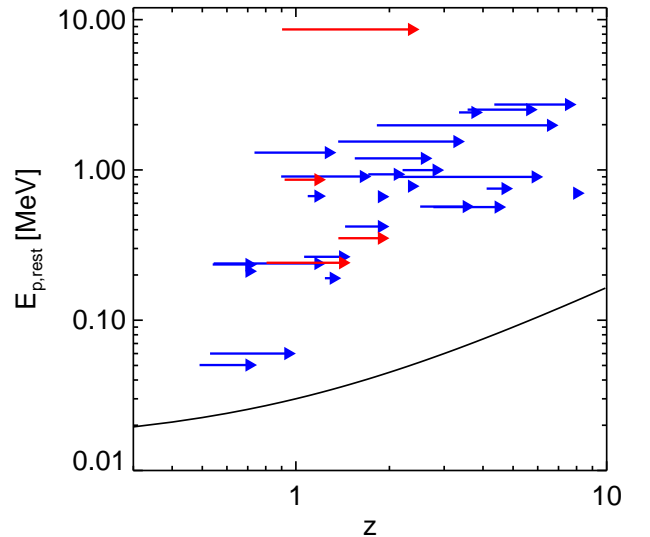


Fig. 11. Same as Fig. 10 but with a line indicating the maximum possible redshift, z_{max} that these 30 GRBs can have to still be detectable by GBM.

4.4.1. Low number statistics?

Another way to test if the $E_p - z$ correlation is genuine is by bearing in mind that it arises simply due to the lack of GRBs with measured redshift and $E_p < 100$ keV. In the present redshift sample there are only 4 GRBs with such a low E_p value. Considering the E_p distribution for 488 GBM bursts of the first two years of operations (Fig. 2) it is possible to estimate as to how many bursts with $E_p < 100$ keV are expected if 32 GRBs are drawn randomly from the full GBM sample. After a run of 10^4 drawings, a distribution is obtained which peaks at ~ 7 . This means that, on average, 7 out of 32 GRBs are expected to have $E_p < 100$ keV. According to our simulation the probability of observing only 4 such GRBs, as we do in our actual sample, is $P = 8\%$, which is within the 2σ limit and thus not significant. Therefore, more GRBs with redshift measurement are required to understand if the “blank area” at low E_p values between $2 < z < 5$ in Fig. 10 is simply underrepresented or not populated at all.

5. Summary & Conclusions

The *Fermi*/GBM is a key instrument to study the temporal and spectral properties of GRBs. For bursts which have redshift measurements it becomes even more important since it allows GRBs to be studied in their rest-frame. Here, we presented such a study for 32 GRBs observed by GBM, focusing on both the temporal and spectral properties, as well as on intra-parameter relations within these quantities.

The $E_{p,\text{rest}}$ distribution of the GBM GRB sample covers an energy range from tens of keV up to several MeV, peaking at ≈ 800 keV. Despite the broader energy coverage of GBM compared to BATSE, no high- E_p population is found. However, the GBM E_p distribution is strongly biased against XRFs or XRBs which have E_p values that fall below 15 keV. Additionally, we confirm a previously reported parameter reconstruction effect, namely that the low-energy power law index α tends to get softer when E_p is close to the lower end of the detector energy range.

Using the canonical internal shock model for GRBs, the mean $E_{p,\text{rest}}$ (≈ 800 keV) implies a dissipation radius of $r_{13} \approx 1.3 L_{52}^{1/2}$ cm.

Another finding of this work is that the width of the E_p distribution is, in fact, not close to zero. Such a claim has recently been brought forward by Collazzi et al. (2011) who argue that all GRBs are thermostated and thus, have the same $E_{p,\text{rest}}$. If true, this would require an unknown physical mechanism that holds GRBs at a constant $E_{p,\text{rest}}$ value. However, it could be shown here that such a mechanism is not required because our sample has an $E_{p,\text{rest}}$ distribution that ranges over several decades in energy.

We find that the $T_{90,\text{rest}}$ stretches from tenths of a second to several hundreds of seconds with a median value of ≈ 10 s.

The E_{iso} distribution ranges from 10^{51} erg to 10^{55} erg, peaking at $\approx 10^{53}$ erg. We confirm the $E_{p,\text{rest}} - E_{\text{iso}}$ correlation and find a power law index of 0.5, consistent with the values reported in the literature but with a significantly larger scatter around the best-fit. We also confirm a strong correlation between the 1 s peak luminosity of the burst and its $E_{p,\text{rest}}$ with a best-fit power law index of 0.57.

We looked for additional correlations between the parameters. We did not find any evidence for a cosmic evolution of $T_{90,\text{rest}}$. Although a correlation between $E_{p,\text{rest}}$ and z is not entirely unexpected from theoretical considerations and looks in-

triguing on a $E_p - z$ plot, we conclude that the apparent relationship is simply arising due to the detector sensitivity.

Acknowledgements. We thank Jonathan Granot for useful discussions. AJvdH was supported by NASA grant NNN07ZDA001-GLAST. SF acknowledges the support of the Irish Research Council for Science, Engineering and Technology, cofunded by Marie Curie Actions under FP7. The GBM project is supported by the German Bundesministerium für Wirtschaft und Technologie (BMWi) via the Deutsches Zentrum für Luft- und Raumfahrt (DLR) under the contract numbers 50 QV 0301 and 50 OG 0502.

References

- Amati, L. 2010, astro-ph:1002.2232
 Amati, L., Frontera, F., Tavani, M., et al. 2002, A&A, 390, 81
 Amati, L., Guidorzi, C., Frontera, F., et al. 2008, MNRAS, 391, 577
 Atwood, W. B., Abdo, A. A., Ackermann, M., et al. 2009, ApJ, 697, 1071
 Band, D., Matteson, J., Ford, L., et al. 1993a, ApJ, 413, 281
 Band, D., Matteson, J., Ford, L., et al. 1993b, ApJ, 413, 281
 Barraud, C., Olive, J., Lestrade, J. P., et al. 2003, A&A, 400, 1021
 Berger, E. 2010, ApJ, 722, 1946
 Berger, E., Fox, D. B., Cucchiara, A., & Cenko, S. B. 2008, GCN, 8335, 1
 Berger, E. & Rauch, M. 2008, GCN, 8542, 1
 Bissaldi, E., von Kienlin, A., Kouveliotou, C., et al. 2011, astro-ph: 1101.3325
 Boella, G., Butler, R. C., Perola, G. C., et al. 1997, A&AS, 122, 299
 Brainerd, J. J., Pendleton, G. N., Mallozzi, R. S., Briggs, M. S., & Preece, R. D. 2000, in American Institute of Physics Conference Series, Vol. 526, Gamma-ray Bursts, 5th Huntsville Symposium, ed. R. M. Kippen, R. S. Mallozzi, & G. J. Fishman, 150–154
 Butler, N. R., Bloom, J. S., & Poznanski, D. 2010, ApJ, 711, 495
 Butler, N. R., Kocevski, D., Bloom, J. S., & Curtis, J. L. 2007, ApJ, 671, 656
 Cash, W. 1979, ApJ, 228, 939
 Cenko, S. B., Bloom, J. S., Morgan, A. N., & Perley, D. A. 2009a, GCN, 9053
 Cenko, S. B., Perley, D. A., Jankkarinen, V., et al. 2009b, GCN, 9518
 Chornock, R., Perley, D. A., Cenko, S. B., & Bloom, J. S. 2009a, GCN, 9028
 Chornock, R., Perley, D. A., Cenko, S. B., & Bloom, J. S. 2009b, GCN, 9243
 Collazzi, A. C., Schaefer, B. E., & Moree, J. A. 2011, ApJ, 729, 89
 Crider, A., Liang, E. P., Smith, I. A., et al. 1997, ApJ, 479, L39+
 Cucchiara, A., Fox, D., Levan, A., & Tanvir, N. 2009a, GCN, 10202, 1 (2009), 202
 Cucchiara, A., Fox, D., & Tanvir, N. 2009b, GCN, 1065, 1 (2009), 65
 Cucchiara, A. & Fox, D. B. 2008, GCN, 8304
 Cucchiara, A. & Fox, D. B. 2010, GCN, 10606, 1 (2010), 606
 Cucchiara, A., Fox, D. B., Cenko, S. B., & Berger, E. 2008, GCN, 8713, 1
 Cucchiara, A., Fox, D. B., Cenko, S. B., Tanvir, N., & Berger, E. 2009c, GCN, 1031, 1 (2009), 31
 Cucchiara, A., Fox, D. B., Tanvir, N., & Berger, E. 2009d, GCN, 9873
 Daigne, F., Rossi, E. M., & Mochkovitch, R. 2006, MNRAS, 372, 1034
 D’Avanzo, P., D’Elia, V., & Covino, S. 2008, GCN, 8350, 1
 de Ugarte Postigo, A., Gorosabel, J., Malesani, D., Fynbo, J. P. U., & Levan, A. J. 2009a, GCN, 9383
 de Ugarte Postigo, A., Jakobsson, P., Malesani, D., et al. 2009b, GCN, 8766, 1
 Fynbo, J. P. U., Malesani, D., Hjorth, J., Sollerman, J., & Thoene, C. C. 2008, GCN, 8254
 Fynbo, J. P. U., Malesani, D., Jakobsson, P., & D’Elia, V. 2009, GCN, 9947
 Gehrels, N., Chincarini, G., Giommi, P., et al. 2004, ApJ, 611, 1005
 Ghirlanda, G., Nava, L., & Ghisellini, G. 2010, A&A, 511, A43+
 Ghirlanda, G., Nava, L., Ghisellini, G., Celotti, A., & Firmani, C. 2009, A&A, 496, 585
 Greiner, J. 2011, astro-ph: 1102.0472
 Greiner, J., Clemens, C., Krühler, T., et al. 2009, A&A, 498, 89
 Gruber, D., Krühler, T., Foley, S., et al. 2011, A&A, 528, A15+
 Harris, M. J. & Share, G. H. 1998, ApJ, 494, 724
 Heise, J. & in ’t Zand, J. 2001, astro-ph: 0112353
 Kaneko, Y., Preece, R. D., Briggs, M. S., et al. 2006, ApJS, 166, 298
 Kann, D. A., Klose, S., Zhang, B., et al. 2008, astro-ph: 0804.1959
 Kippen, R. M., in ’t Zand, J. J. M., Woods, P. M., et al. 2004, in American Institute of Physics Conference Series, Vol. 727, Gamma-Ray Bursts: 30 Years of Discovery, ed. E. Fenimore & M. Galassi, 119–122
 Kouveliotou, C., Meegan, C. A., Fishman, G. J., et al. 1993, ApJ, 413, L101
 Levan, A. J., Fynbo, J. P. U., Hjorth, J., et al. 2009, GCN, 9958
 Lloyd, N. M. & Petrosian, V. 2000, ApJ, 543, 722
 Lloyd-Ronning, N. M. & Petrosian, V. 2002, ApJ, 565, 182
 Malesani, D., Goldoni, P., Fynbo, J. P. U., et al. 2009, GCN, 9942
 Markwardt, C. B., Barthelmy, S. D., Baumgartner, W. H., et al. 2010, GCN, 11111, 1 (2010), 1111
 Meegan, C., Lichti, G., Bhat, P. N., et al. 2009, ApJ, 702, 791

- Meegan, C. A., Fishman, G. J., Wilson, R. B., et al. 1992, *Nature*, 355, 143
Nava, L., Ghirlanda, G., Ghisellini, G., & Celotti, A. 2010, *astro-ph*: 1012.3968
Norris, J. P. & Bonnell, J. T. 2006, *ApJ*, 643, 266
O'Meara, J., Chen, H., & Prochaska, J. X. 2010, *GCN*, 11089, 1 (2010), 1089
Pélangeon, A., Atteia, J., Nakagawa, Y. E., et al. 2008, *A&A*, 491, 157
Preece, R. D., Briggs, M. S., Malozzi, R. S., et al. 1998, *ApJ*, 506, L23
Prochaska, J. X., Perley, D., Howard, A., et al. 2008, *GCN*, 8083
Rau, A., McBreen, S., & Kruehler, T. 2009, *GCN*, 9353
Rossi, A., Afonso, P., & Greiner, J. 2009a, *GCN*, 9382
Rossi, A., Kruehler, T., Greiner, J., & Yoldas, A. 2009b, *GCN*, 9408
Sakamoto, T., Lamb, D. Q., Kawai, N., et al. 2005, *ApJ*, 629, 311
Sakamoto, T., Sato, G., Barbier, L., et al. 2009, *ApJ*, 693, 922
Salvatterra, R. & Chincarini, G. 2007, *ApJ*, 656, L49
Salvatterra, R., Guidorzi, C., Campana, S., Chincarini, G., & Tagliaferri, G. 2009, *MNRAS*, 396, 299
Tanvir, N. R., Fox, D. B., Levan, A. J., et al. 2009, *Nature*, 461, 1254
Tanvir, N. R., Vergani, S., Hjorth, J., et al. 2010, *GCN*, 11123, 1 (2010), 1123
Thoene, C. C., de Ugarte Postigo, A., Vreeswijk, P. M., Malesani, D., & Jakobsson, P. 2008, *GCN*, 8058, 1
Thoene, C. C., Jakobsson, P., de Cia, A., et al. 2009, *GCN*, 9409
Vreeswijk, P. M., Fynbo, J. P. U., Malesani, D., Hjorth, J., & de Ugarte Postigo, A. 2008, *GCN*, 8191
Wang, F. Y. & Dai, Z. G. 2011, *ApJ*, 727, L34+
Wiersema, K., de Ugarte Postigo, A., & Levan, A. 2009a, *GCN*, 9250
Wiersema, K., Tanvir, N. R., Cucchiara, A., Levan, A. J., & Fox, D. 2009b, *GCN*, 10263, 1 (2009), 263
Xu, D., Fynbo, J. P. U., Tanvir, N. R., et al. 2009, *GCN*, 1053, 1 (2009), 53
Yonetoku, D., Murakami, T., Nakamura, T., et al. 2004, *ApJ*, 609, 935
Zhang, B. & Mészáros, P. 2002, *ApJ*, 581, 1236
Zhang, B., Zhang, B., Virgili, F. J., et al. 2009, *ApJ*, 703, 1696

Table 2. Rest-frame parameters of 32 GBM GRBs.

GRB	Mission	$T_{90,\text{rest}}$ [s]	$E_{p,\text{rest}}$ [keV]	Best Fitting Model	z	Ref.
100816A	Swift	1.11 ± 0.11	241^{+11}_{-11}	BAND	0.8049(1)	[1]
100814A	Swift	60.25 ± 0.90	420^{+23}_{-21}	COMP	1.44(1)	[2]
100414A	Swift	9.42 ± 0.21	1544^{+31}_{-31}	COMP	1.368(1)	[3]
100117	Swift	0.17 ± 0.07	861^{+595}_{-152}	COMP	0.92(1)	[4]
091208B	Swift	5.82 ± 0.19	264^{+24}_{-20}	COMP	1.063(1)	[5]
091127	Swift	5.37 ± 0.20	50^{+3}_{-3}	BAND	0.490(1)	[6]
091024 ^a	Swift	≈ 487.80	659^{+90}_{-67}	COMP	1.092(1)	[7]
091020	Swift	14.54 ± 1.18	935^{+213}_{-140}	BAND	1.71(1)	[8]
091003A	Fermi	10.91 ± 0.16	904^{+39}_{-36}	COMP	0.8969(1)	[9]
090927	Swift	0.42 ± 0.04	351^{+96}_{-63}	COMP	1.37(1)	[10]
090926B	Swift	45.27 ± 2.05	190^{+6}_{-6}	COMP	1.24(1)	[11]
090926A	Fermi	4.44 ± 0.06	898^{+17}_{-16}	BAND*	2.1062(1)	[12]
090902B	Fermi	6.80 ± 0.11	1980^{+26}_{-25}	COMP+PL	1.822(1)	[13]
090618	Swift	72.66 ± 0.45	235^{+5}_{-4}	BAND*	0.54(1)	[14]
090519A	Swift	10.76 ± 4.06	...	PL	3.85(1)	[15, 16]
090516A	Swift	43.49 ± 3.70	751^{+83}_{-67}	COMP	4.109(1)	[17, 18]
090510	Swift	0.63 ± 0.11	8605^{+660}_{-592}	BAND+PL	0.903(1)	[19]
090424	Swift	10.10 ± 0.39	239^{+5}_{-5}	BAND	0.544(1)	[20, 21]
090423	Swift	3.19 ± 0.16	700^{+154}_{-96}	COMP	8.26(8)	[22]
090328A	Fermi	31.74 ± 0.58	1304^{+93}_{-83}	COMP	0.736(1)	[23]
090323	Fermi	28.91 ± 0.13	2518^{+135}_{-131}	BAND	3.57(1)	[24]
090102	Swift	10.56 ± 0.27	1194^{+60}_{-55}	COMP	1.547(1)	[25]
081222	Swift	5.78 ± 0.48	566^{+39}_{-35}	BAND	2.77(1)	[26]
081121	Swift	5.30 ± 0.46	570^{+61}_{-52}	BAND	2.512(1)	[27]
081008	Swift	48.64 ± 6.80	664^{+130}_{-94}	COMP	1.9685(1)	[28]
081007	Swift	7.19 ± 1.31	60^{+9}_{-9}	COMP	0.5295(1)	[29]
080928	Swift	17.42 ± 2.30	...	PL	1.692(1)	[30]
080916C	Fermi	18.37 ± 2.13	2724^{+177}_{-138}	BAND	4.35(5)	[31]
080916A	Swift	20.49 ± 0.36	212^{+14}_{-12}	COMP	0.689(1)	[32]
080905B	Swift	28.96 ± 0.59	779^{+246}_{-153}	COMP	2.374(1)	[33]
080810	Swift	13.75 ± 1.10	2413^{+32}_{-258}	BAND	3.35(1)	[34]
080804	Swift	6.12 ± 0.56	997^{+104}_{-86}	COMP	2.2045(1)	[35]

Notes. The columns show the name of the GRB, $T_{90,\text{rest}}$, $E_{p,\text{rest}}$, best fitting model, redshift and redshift references of the 32 GBM GRBs presented here. The keyword “Swift” in the mission column denotes whether the GRB triggered both *Swift* and GBM, whereas “Fermi” indicates that it was triggered by GBM only.

For bursts with * an effective area correction was applied to the BGO with respect to the NaI detectors.

^(a) The $T_{90,\text{rest}}$ and $E_{p,\text{rest}}$ values for GRB 091024 were taken from Gruber et al. (2011)

References. (1) Tanvir et al. (2010) ; (2) O’Meara et al. (2010) ; (3) Cucchiara & Fox (2010) ; (4) Berger (2010) ; (5) Wiersema et al. (2009b) ; (6) Cucchiara et al. (2009a) ; (7) Cucchiara et al. (2009b) ; (8) Xu et al. (2009) ; (9) Cucchiara et al. (2009c) ; (10) Levan et al. (2009) ; (11) Fynbo et al. (2009) ; (12) Malesani et al. (2009) ; (13) Cucchiara et al. (2009d) ; (14) Cenko et al. (2009b) ; (15) Thoene et al. (2009) ; (16) Rossi et al. (2009b) ; (17) de Ugarte Postigo et al. (2009a) ; (18) Rossi et al. (2009a) ; (19) Rau et al. (2009) ; (20) Chornock et al. (2009b) ; (21) Wiersema et al. (2009a) ; (22) Tanvir et al. (2009) ; (23) Cenko et al. (2009a) ; (24) Chornock et al. (2009a) ; (25) de Ugarte Postigo et al. (2009b) ; (26) Cucchiara et al. (2008) ; (27) Berger & Rauch (2008) ; (28) D’Avanzo et al. (2008) ; (29) Berger et al. (2008) ; (30) Cucchiara & Fox (2008) ; (31) Greiner et al. (2009) ; (32) Fynbo et al. (2008) ; (33) Vreeswijk et al. (2008) ; (34) Prochaska et al. (2008) ; (35) Thoene et al. (2008) .